

#### **STAP ARTICLE**

# Fabrication of ceramic scintillators by laser sintering: the case of ${\rm Lu_3Al_5O_{12}}$ :Pr

To cite this article: Y. Shao et al 2023 Jpn. J. Appl. Phys. 62 010601

View the article online for updates and enhancements.

## You may also like

- Na<sub>2</sub>O-Gd<sub>2</sub>O<sub>3</sub>-Al<sub>2</sub>O<sub>3</sub>-P<sub>2</sub>O<sub>5</sub> glass scintillator doped with Dy<sup>3+</sup>: X-rays and proton responses

responses
Nuanthip Wantana, Eakgapon Kaewnuam,
Yaowaluk Tariwong et al.

- <u>High pressure luminescence spectra of CaMoO<sub>4</sub>:Ln<sup>3+</sup> (Ln = Pr, Tb) S Mahlik, M Behrendt, M Grinberg et al.</u>
- <u>Pressure-induced phase transition in LiLuF\_:Pr<sup>3+</sup> investigated by an optical technique</u>

A Lazarowska, S Mahlik, M Krosnicki et al.

Recent advances in radiation-induced luminescence materials

# Check for updates

### Fabrication of ceramic scintillators by laser sintering: the case of Lu<sub>3</sub>Al<sub>5</sub>O<sub>12</sub>:Pr

Y. Shao<sup>1</sup>, R. L. Conner<sup>1</sup>, N. R. S. Souza<sup>2</sup>, R. S. Silva<sup>2</sup>, and L. G. Jacobsohn<sup>1,3\*</sup>

<sup>1</sup>Department of Materials Science and Engineering, Clemson University, Clemson SC 29634, United States of America

\*E-mail: luiz@clemson.edu

Received September 2, 2022; revised October 5, 2022; accepted October 10, 2022; published online November 22, 2022

The fabrication of ceramic scintillators by laser sintering is briefly reviewed and current limitations discussed. The experimental work focused on the fabrication and characterization of undoped and Pr-doped Lu<sub>3</sub>Al<sub>5</sub>O<sub>12</sub> (LuAG). X-ray diffraction (XRD) and Raman spectroscopy were used to characterize the structure of the sintered ceramics, with XRD results suggesting the absence of residual thermal stresses. Collectively, Raman results suggested the incorporation of Pr to affect the structure and its dynamics. Broadening the peaks of the ceramics in relation to those from the single crystal revealed the presence of structural disorder. Scanning electron microscopy revealed intergrain porosity thus explaining the lack of optical transparency. Energy-dispersive X-ray spectroscopy (EDX) measurements showed Pr to be homogeneously distributed. Radioluminescence measurements under X-ray excitation as a function of the temperature were used to investigate intrinsic defects of the host, including anti-sites and F-type defects. © 2022 The Japan Society of Applied Physics

#### 1. Introduction

Laser sintering is a novel method first introduced in the late 1980s for the fabrication of dense ceramic bodies. It presents significant advantages when compared to conventional sintering, especially spatially localized sintering and high heating and cooling rates, in addition to short sintering times of minutes compared to several hours needed by conventional sintering.<sup>1)</sup> Starting in the early 2000s, this method has been applied to the fabrication of optical materials with a particular focus on scintillators and persistent phosphors. The intrinsic scintillator Bi<sub>4</sub>Ge<sub>3</sub>O<sub>12</sub> (BGO) was the first to be fabricated by laser sintering. <sup>2–4)</sup> Later, doped phosphors were also fabricated, including  $Y_2O_3^{5}$  and  $Y_3Al_5O_5$  (YAG),  $^{6-10)}$ concomitant to an intense effort focused on aluminate-based persistent phosphors. 11-15) Overall, high densities, typically ≥95% of the theoretical density were obtained, the achievement of optical transparency remains a challenge.

In addition to optical transparency, another major concern for optical materials is the distribution of dopants in the sintered materials. The first in-depth investigations of dopant homogeneity were carried out on the laser-sintered persistent phosphors SrAl<sub>2</sub>O<sub>4</sub>:Eu,Dy<sup>11)</sup> and CaAl<sub>2</sub>O<sub>4</sub>:Eu,Dy. <sup>13)</sup> While optical translucency in these materials was achieved, Eu and Dy segregated in the grain boundaries as determined by elemental mapping and line scans obtained by energydispersive X-ray spectroscopy (EDX) measurements. Considerable effort was also directed in the fabrication of rare earth doped YAG, including phosphor and scintillator YAG:Ce.<sup>9,10)</sup> The detection of gamma-rays with a lasersintered YAG:Ce ceramic was demonstrated. 10) While YAG: Ce was the first laser-sintered garnet investigated as scintillator, Lu<sub>3</sub>Al<sub>5</sub>O<sub>12</sub> (LuAG) is an attractive option due to its higher density and effective atomic number, and several rare earths have been proposed as activators for this host. 16)

In terms of activators among the rare earths, it is interesting to note that the ionic radius can play an important role in the fabrication of doped materials. For example, the incorporation of Tb ions into YAG can be considered straightforward due to the small relative difference of 2% in ionic radii between eightfold coordinated  $Y^{3+}$  ( $R_Y = 1.019$  Å<sup>17)</sup>) and

 $\text{Tb}^{3+}$  ( $R_{\text{Tb}} = 1.04 \text{ Å}^{17}$ ). On the other hand, in the case of Pr doping of LuAG, the relative difference in ionic radii between eightfold coordinated  $Pr^{3+}$  ( $R_{Pr} = 1.126 \text{ Å}^{17}$ ) and  $Lu^{3+}$  ( $R_{Lu} = 0.977$  Å<sup>17</sup>) is 15%. This relatively large difference resulted in a large variation of the Pr concentration along the boule and the formation of inclusions of a Pr-Al-O phase at the end of the boule in Czochralski-grown LuAG:Pr single crystals. <sup>18)</sup> Since materials fabricated by laser sintering are affected by high heating and cooling rates that are far from the thermodynamic equilibrium, it is conceivable that higher levels of Pr incorporation into LuAG can be achieved. Within this context, the effort to fabricate ceramic scintillators by laser sintering was expanded and a first attempt to fabricate undoped and Pr-doped LuAG ceramics using laser sintering was executed. The ceramic bodies were characterized by their structure and luminescence properties in comparison to results from conventional sintering 19,20) and a Czochralski-grown LuAG:Pr single crystal.<sup>20)</sup> Since laser sintering operates at such unique thermodynamic conditions, special attention was paid to the identification of the defects created in the ceramic host.

#### 2. Experimental methods

Powders of (Lu<sub>0.99</sub>Pr<sub>0.01</sub>)<sub>3</sub>Al<sub>5</sub>O<sub>12</sub> were obtained by a coprecipitation method. 19) Lutetium nitrate was obtained by dissolving commercial Lu<sub>2</sub>O<sub>3</sub> (99.995%, HEFA Rare Earth Canada Co.) in excess of 70% nitric acid (Certified A.C.S., Spectrum) while stirring and heating. Aluminum nitrate (98%, Alfa Aesar) and praseodymium nitrate (99.9%, Acros Organics) were dissolved in ultrapure water at room temperature (RT) in a separate beaker and added drop-wise to the stirring lutetium nitrate solution after it cooled down to RT. The mixed nitrate solution was added drop-wise to a 1:1 solution of ultrapure water and ammonium hydroxide (Certified A.C.S Plus, Fisher Scientific) towards the precipitation of LuAG:Pr. The precipitate was allowed to stir at RT for 1 h and then washed three times with ultrapure water and twice with ethanol before being dried at 60 °C overnight in vacuum. X-ray diffraction (XRD) measurements revealed that the precipitates were not LuAG:Pr, and calcination in air at 1000 °C for 2 h in an alumina boat was carried out.<sup>19)</sup>

<sup>&</sup>lt;sup>2</sup>Physics Department, Federal University of Sergipe, 49100-000 Sao Cristovao, SE, Brazil

<sup>&</sup>lt;sup>3</sup>Center for Nuclear Environmental Engineering Sciences and Radioactive Waste Management (NEESRWM), Clemson University, Anderson SC 29625, United States of America

Energy-dispersive X-ray spectroscopy (EDX) measurements revealed the Pr concentration to be 0.18 at% in relation to the whole composition against the nominal value of 0.15 at%. <sup>19)</sup> A LuAG:Pr single crystal grown by the Czochralski method was used in Ref. 21. Laser sintering <sup>8,9)</sup> was done on 4 mm diameter pellets obtained by uniaxially pressing the powders at 100 MPa. The pellets were sintered using a CO<sub>2</sub> laser (GEM-100L–Coherent) in continuous wave mode as the heating source. The laser power was increased linearly to a maximum power density of 2.8 W mm<sup>-2</sup> with a dwell time of 90 s and this process was executed on both faces.

Scanning electron microscopy (SEM) imaging, EDX mapping and EDX line scanning were executed using a Hitachi SU5000 variable pressure scanning electron microscope operating at 20 kV and 30 Pa in backscattered electron (BSE) mode.

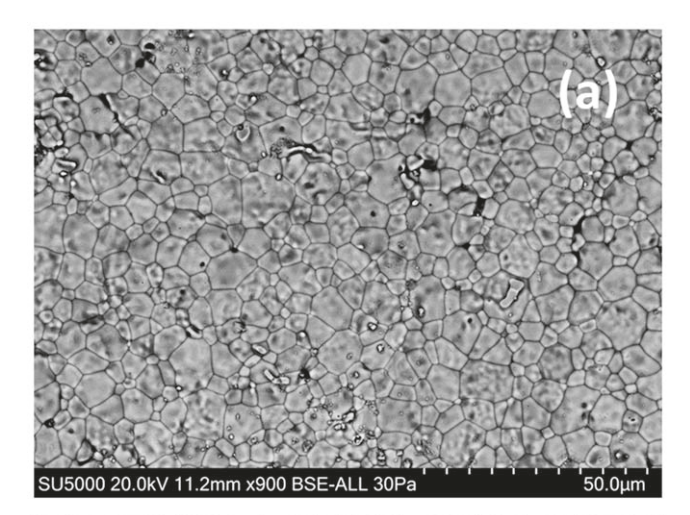
XRD measurements were executed using a Rigaku Ultima IV X-ray diffractometer with non-filtered Cu K radiation with a step size of  $0.01^{\circ}$ .

Raman scattering spectroscopy was executed with a Horiba LabRAM HR Evolution Raman microscope equipped with a 800 mm focal length spectrograph and a cooled ( $-60^{\circ}$  C) back-illuminated deep-depleted  $1024 \times 256$  pixels CCD detector using a frequency doubled YAG:Nd laser at 532 nm and 600 groves mm<sup>-1</sup> diffraction gratings. Each spectrum was corrected by the pre-recorded instrument-specific response to a calibrated white light source, namely the intensity correction system.

Radioluminescence (RL) measurements were carried out using a customer-designed configuration of the Freiberg Instruments Lexsyg spectrofluorometer equipped with a Varian Medical Systems VF-50J X-ray tube with a tungsten target. The X-ray source was coupled with a Crystal Photonics CXD-S10 photodiode for continuous radiation intensity monitoring. The light emitted by the sample was collected by an Andor Technology SR-OPT-8024 optical fiber connected to an Andor Technology Shamrock 163 spectrograph coupled to a cooled (-80 °C) Andor Technology DU920P-BU Newton CCD camera (spectral resolution of  $\sim 0.5$  nm/pixel). RL was measured under continuous X-ray irradiation (W lines and bremsstrahlung radiation; 40 kV, 1 mA) with an integration time of 1 s. Selected RL measurements as a function of the temperature were executed under continuous heating with a 1 °C s<sup>-1</sup> heating rate up to 400 °C and a 5 s integration time. Thus, temperature increased by 5 °C during the acquisition of each spectrum. Spectra were labeled by the starting acquisition temperature and were automatically corrected using the spectral response of the system determined by the manufacturer.

#### 3. Results and discussion

The ceramics were characterized on their morphology, structure, and chemical homogeneity. The morphology of both undoped and Pr-doped ceramics is illustrated in Fig. 1 where numerous polygonal grains with sizes ranging within about  $1-15~\mu m$  can be seen. No significant difference between the undoped and Pr-doped ceramics was observed. For comparison, average grain sizes of LuAG:Pr ceramics prepared by conventional sintering from 1400 °C to 1700 °C have grain sizes of about  $0.4-2~\mu m$ . The formation of



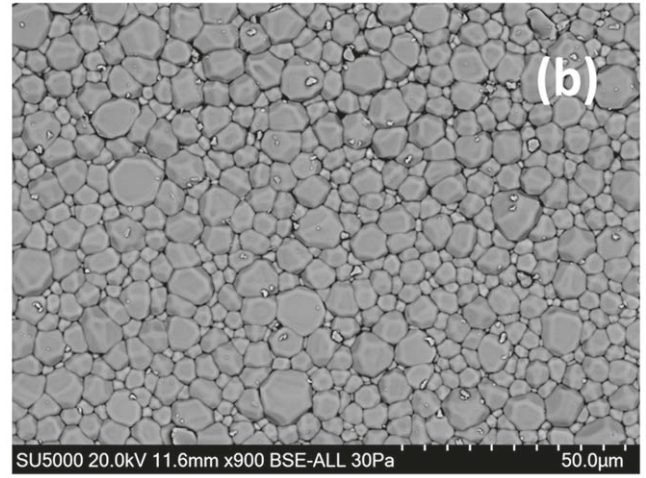


**Fig. 1.** SEM images of (a) undoped, and (b) Pr-doped laser-sintered LuAG ceramics.

considerably large grains in the case of the laser-sintered ceramics suggests a particularly fast growth mechanism and intense atomic transport. The presence of intergrain porosity was evident and that explained the lack of optical transparency of the ceramics.

The XRD diffractograms of the undoped and Pr-doped ceramics were indexed to the cubic phase of Lu<sub>3</sub>Al<sub>5</sub>O<sub>12</sub> with space group Ia 3d (230) according to the ICDD PDF Card No.: 01-073-1368, and no additional phases were observed. These results are illustrated in Fig. 2 for the undoped ceramic together with the Lu<sub>3</sub>Al<sub>5</sub>O<sub>12</sub> PDF card (bar plot). The average lattice parameter was calculated based on the (321), (420) and (532) diffraction peaks and matched the value from the PDF file with relative difference better than 0.3% suggesting the absence of significant residual thermal stresses originating from laser sintering.

The unit cell of cubic  $Lu_3Al_5O_{12}$  contains eight molecular units with the structure being composed of dodecahedral sites occupied by Lu and Pr, and tetrahedral and octahedral sites occupied by Al. Figure 3 shows a comparison of the Raman spectra of the undoped and Pr-doped ceramics with that of the LuAG:Pr single crystal. All the vibrational modes were identified based on the work by Song et al. A systematic shift of  $\sim$ 7 cm<sup>-1</sup> to lower wavenumbers was observed in the spectra obtained in this work and attributed to the fact that these measurements were obtained at RT while those from

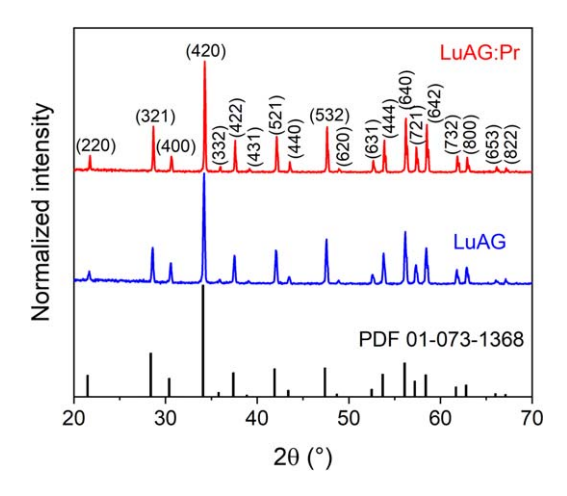


**Fig. 2.** (Color online) Normalized XRD diffractograms of undoped and Prdoped laser-sintered ceramics indexed according to PDF file no. 01-073-1368. The diffractograms were shifted vertically for visual clarity.

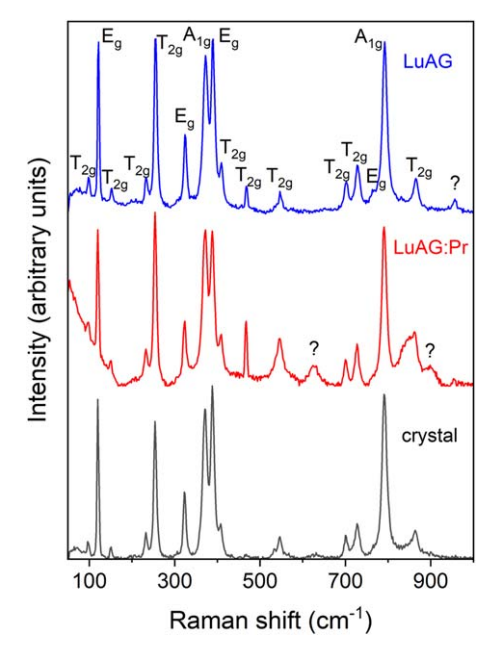


**Fig. 3.** (Color online) Comparison between the Raman spectra of undoped and Pr-doped LuAG ceramics with that of a LuAG:Pr single crystal. The spectra were shifted vertically for visual clarity.

Ref. 22 were obtained at 80 K. Indeed, lower temperatures are expected to cause a contraction of chemical bonds and thus an increase of the corresponding vibrational frequencies. Most vibrational peaks could be matched with the results from Ref. 22, with the first three at 97, 120 and 151 cm<sup>-1</sup> attributed to the translational mode of Lu3+ ions and the peaks within 500-900 cm<sup>-1</sup> to different vibrational modes of the AlO<sub>4</sub> tetrahedra.<sup>23)</sup> Noticeably, the peak at 468 cm<sup>-1</sup> is considerably more intense in the case of the ceramics than in the single crystal. On the other hand, the peak at 627 cm<sup>-1</sup> observed in the Pr-doped ceramic and the single crystal, the peak at 898 cm<sup>-1</sup> observed in the Pr-doped ceramic, and the peak at 957 cm<sup>-1</sup> observed in the undoped ceramic could not be identified. Moreover, the shape of the peak at 864 cm<sup>-1</sup> in the Pr-doped ceramic is much broader than in the undoped ceramic and the single crystal, and perhaps contains a lower frequency shoulder. Collectively, these results suggest that the incorporation of Pr affects the structure and its dynamics.

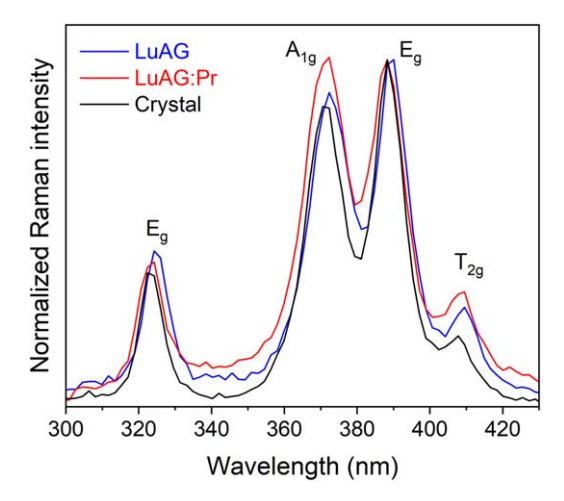


**Fig. 4.** (Color online) Comparison of the width of several vibrational modes at 323, 371, 388 and 408 cm<sup>-1</sup> of the undoped and Pr-doped LuAG ceramics with those of the LuAG:Pr single crystal. Spectra were normalized to the intensity of the  $E_g$  vibrational mode at 408 cm<sup>-1</sup>.

Comparison of the width of the peaks of the ceramics with those of the single crystal revealed a systematic broadening, as illustrated in Fig. 4, indicating the presence of structural disorder in the laser-sintered ceramics.

The homogeneity of the Pr activator was investigated by means of EDX mapping. The concentrations of Al, O and Pr were determined by mapping several regions containing numerous grains as illustrated in Fig. 5. Figure 5(a) presents a SEM image obtained in BSE mode showing the morphology of the laser-sintered ceramic. Figures 5(b) to 5(d) show the corresponding elemental mapping results for Al  $K\alpha 1$ , O  $K\alpha 1$  and Pr  $L\alpha 1$  lines, respectively. It was possible to correlate Fig. 5(a) with Figs. 5(b) to 5(d), though in the case of Pr the correlation was more difficult due to the lower concentration of Pr and thus the lower intensity of its L $\alpha$ 1 line. This correlation was an indication of the homogeneous distribution of the activator concomitant to the absence of indication of grain boundary segregation. This result was further confirmed by line scans crossing from one grain into another, as illustrated in Fig. 6. In Fig. 6, the Pr profile was similar to those of the other elements, with the dip of the concentrations occurring in the intergrain region being the result of topographical features as revealed by the SEM image [Fig. 6(a)].

RL spectra at RT of the undoped and Pr-doped ceramics and of the LuAG:Pr single crystal are presented in Fig. 7. In the case of the Pr-doped materials, spectra are dominated by a double-band within 300-450 nm. This intense double-band is due to the  $Pr^{3+} 5d \rightarrow 4f$  emission and is, in fact, composed by four transitions from the 5d state to the  ${}^{3}F_{3(4)}$ ,  ${}^{3}H_{6}$ ,  ${}^{3}H_{5}$ ,  ${}^{3}H_{4}$ 4f states.<sup>24)</sup> Its intensity is justified by the relative positions of the levels 4  $f^15d^1$  and  ${}^1S_0$  to the conduction band.<sup>25)</sup> Additional emission at higher wavelengths was due to Pr<sup>3+</sup>  $4f \rightarrow 4f$  transitions.<sup>26)</sup> Interestingly, these bands have a better defined shape and are relatively stronger in the ceramic than in the single crystal. This difference was attributed to the structural disorder observed in the ceramic that relaxed Laporte selection rules and facilitated forbidden  $4f \rightarrow 4f$ transitions. On the other hand, undoped LuAG presented different bands than the Pr-doped materials, one within 300-550 nm that comprised several bands, and another starting at

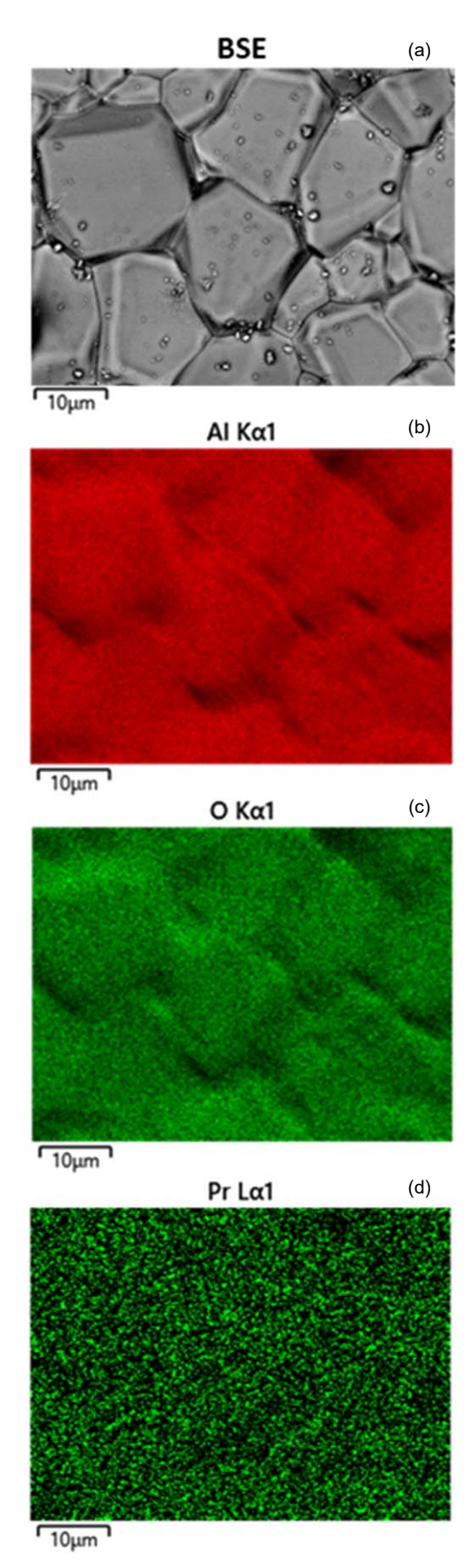
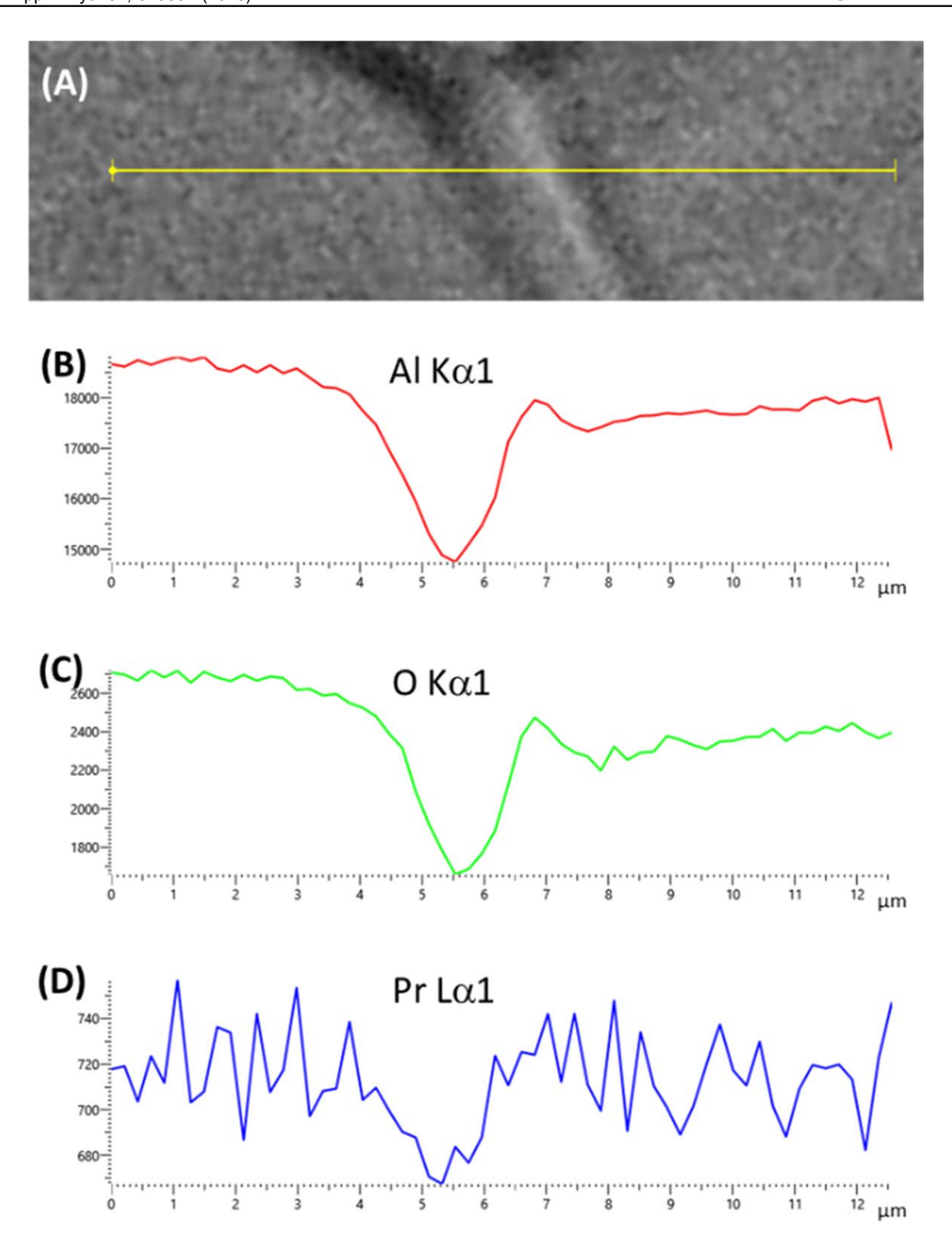


Fig. 5. (Color online) (a) SEM image obtained in BSE mode, and corresponding elemental mapping of (b) Al, (c) O, and (d) Pr.

550 nm that presented four well-defined lines at 672, 685, 704, and 724 nm. These lines were attributed to  $Cr^{3+}$  impurities due to the similarities with YAG:Cr spectra.<sup>27)</sup>

Given the unique thermodynamic conditions in which laser sintering occurs, one of the goals of this work is to investigate how laser sintering affects the relative population of defects



**Fig. 6.** (Color online) (a) SEM image obtained in BSE mode of a grain boundary showing the path of the EDX linear scan and corresponding intensities of (b) Al  $K\alpha 1$ , (c) O  $K\alpha 1$ , and (d) Pr  $L\alpha 1$  lines.

in the LuAG host. Towards this goal, RL measurements as a function of the temperature were executed. It is expected that different defects have different thermal stabilities and that these measurements will yield insight into the nature of the individual bands composing the broad band observed at low wavelengths. This approach was successfully employed in another garnet-type material towards the understanding of Ce<sup>3+</sup> luminescence in that host.<sup>28)</sup> Figure 8 shows spectra within the 2–4.5 eV spectral region obtained at selected

temperatures from RT up to 148 °C after Jacobian transformation. Emission below 2.25 eV was due to Cr³+ contribution. The superposition of several peaks composing the broad emission band was evident from visual inspection and spectral analysis was executed using Gaussian bands. Different combinations of Gaussian bands were used, and best results were obtained with four Gaussian bands (Fig. 9), in agreement with visual inspection of RL spectra at high temperatures. It is noted that at higher temperatures, the

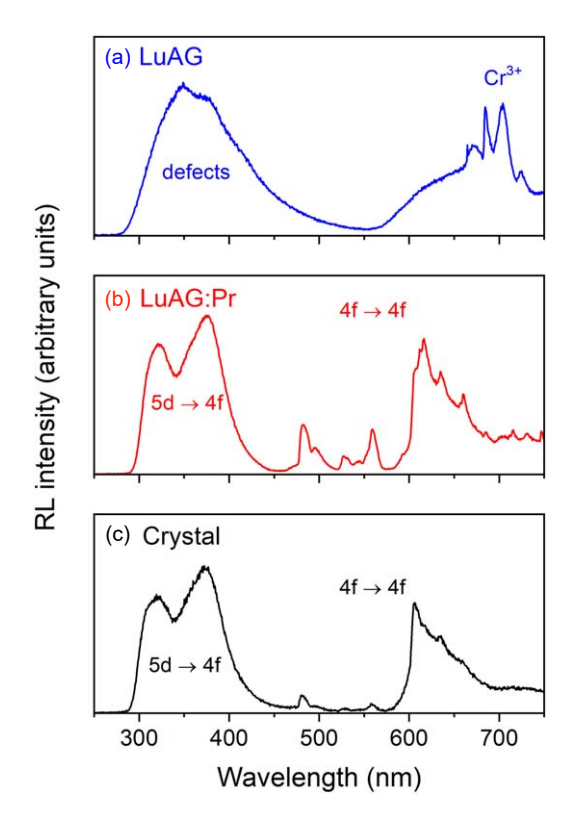


**Fig. 7.** (Color online) RL spectra of (a) undoped and (b) Pr-doped LuAG laser-sintered ceramics, and (c) LuAG:Pr single crystal.

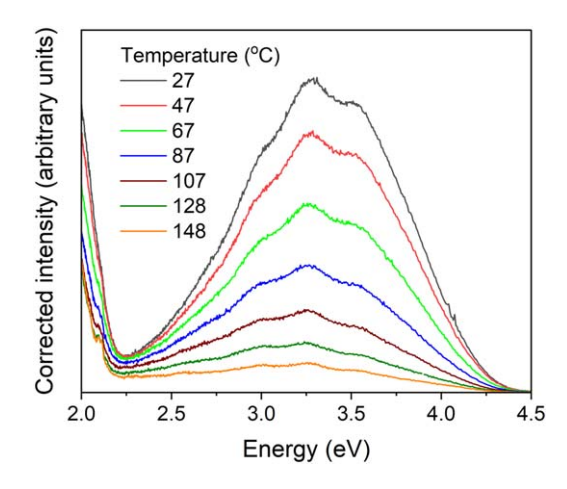
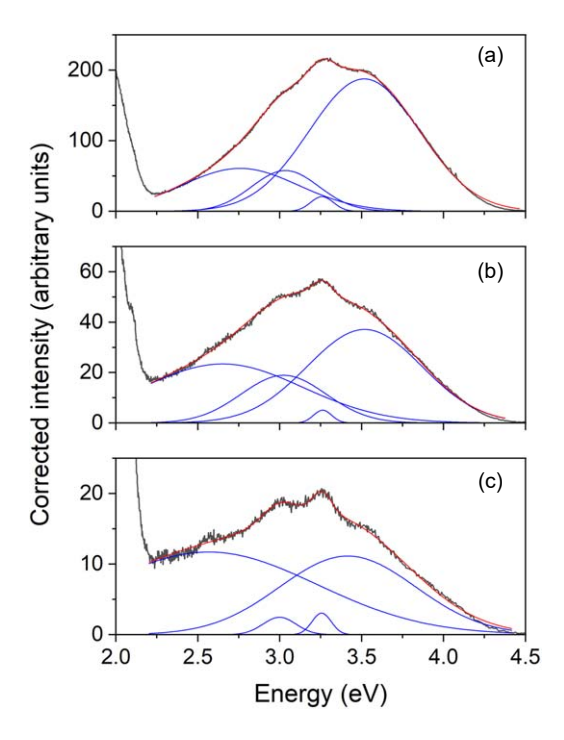
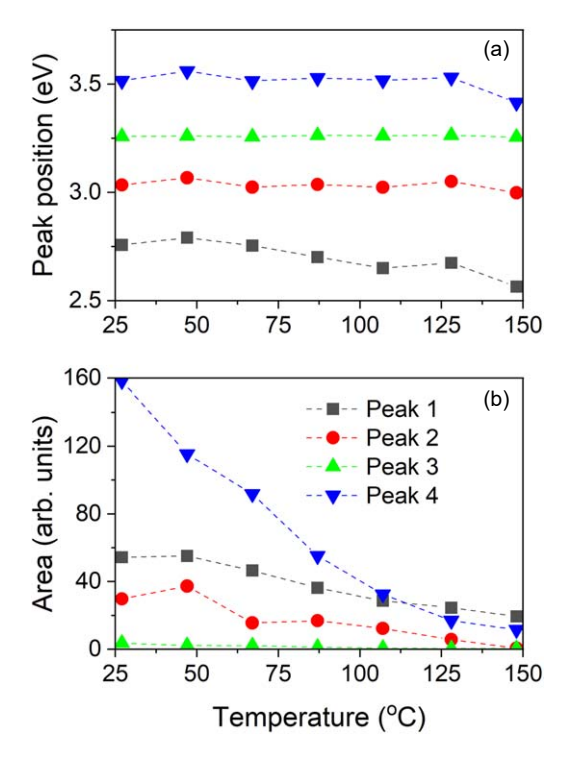


Fig. 8. (Color online) RL spectra of undoped laser-sintered ceramic at selected temperatures.

contribution of the Cr<sup>3+</sup> tail into the spectra was relatively stronger and thus expected to affect the fitting results, especially of peak 1. Nevertheless, a coefficient of determination (R-squared) value of at least 0.99 was obtained in all cases. At RT, the peak positions were 2.79 eV (444 nm; peak 1), 3.03 eV (409 nm; peak 2), 3.26 eV (peak 3), and 3.52 eV (peak 4) with peak 1 shifting to lower energies while the other peak positions remained essentially unchanged. All peak intensities decreased for higher temperatures (Fig. 10). With the exception of peak 1 that was not previously reported, these emissions were in agreement with the literature: emission around 3.0 eV (peak 2) was attributed to F<sup>+</sup>-type defects/oxygen vacancies, <sup>29,30)</sup> and around 3.26 eV (peak 3) to Lu<sub>Al</sub> anti-sites. 31) Emission around 3.5 eV (peak 4) was previously reported but not identified.<sup>30)</sup> Commonly, the electron-phonon coupling of electrons in structural



**Fig. 9.** (Color online) Gaussian fitting results illustrated for RL spectra (black lines) obtained at (a) 27 °C, (b) 107 °C, and (c) 148 °C where blue curves correspond to the individual Gaussian curves and the red line to the cumulative best fit.



**Fig. 10.** (Color online) (a) Peak position and (b) area of the individual Gaussian bands as a function of the temperature.

defects with the vibrations of the structure yield full width at half maximum (FWHM) values around  $0.8 \text{ eV}.^{32,33)}$  The FWHM values of  $\sim 0.5$  to 0.8 eV of peaks 1, 2 and 4 were compatible with the proposed assignments discussed above.

#### 4. Summary and conclusions

Laser sintering stands as a novel promising method for the fabrication of optical ceramics, and especially scintillators.

Well-known scintillators like BGO and YAG:Ce have been fabricated and investigated in their morphology, structure and luminescence, including the demonstration of gamma-ray detection. <sup>10)</sup> In this work, this investigative effort was expanded to include LuAG:Pr. While single phase ceramics were obtained with the Pr activator homogeneously distributed throughout the ceramic body, the lack of optical transparency remains a major issue.

#### **Acknowledgments**

This material is based upon work supported by the National Science Foundation under Grant No. 1653016. The authors are in debt to C. L. Melcher with the Scintillation Materials Research Center, the University of Tennessee, Knoxville, for providing the LuAG:Pr single crystal, and to M. R. Marchewka for the synthesis of the LuAG(:Pr) powders.

#### **ORCID iDs**

- R. S. Silva https://orcid.org/0000-0001-6983-110X L. G. Jacobsohn https://orcid.org/0000-0001-8991-3903
- 1) B. Qian and Z. Shen, J. Asian Ceram. Soc. 1, 315 (2013).
- 2) Z. S. Macedo and A. C. Hernandes, J. Am. Ceram. Soc. 85, 1870 (2002).
- Z. S. Macedo, R. S. Silva, M. E. G. Valerio, A. L. Martinez, and A. C. Hernandes, J. Am. Ceram. Soc. 87, 1076 (2004).
- Z. S. Macedo, R. S. Silva, M. E. G. Valerio, and A. C. Hernandes, Nuc. Instrum. Meth. Phys. Res. B 218, 153 (2004).
- T. C. Oliveira, M. C. Silva, L. M. Jesus, D. V. Sampaio, J. C. A. Santos, N. R. S. Souza, and R. S. Silva, Ceram. Inter. 40, 16209 (2014).
- J. C. A. Santos, E. P. Silva, D. V. Sampaio, N. R. S. Souza, Y. G. S. Alves, and R. S. Silva, Mater. Lett. 160, 456 (2015).
- J. C. A. Santos, E. P. Silva, N. R. S. Souza, Y. G. S. Alves, D. V. Sampaio, C. Kucera, L. G. Jacobsohn, J. Ballato, and R. S. Silva, Ceram. Inter. 45, 3797 (2019).
- J. C. A. Santos, E. P. Silva, D. V. Sampaio, Y. G. S. Alves, M. V. S. Rezende, C. Kucera, J. Ballato, and R. S. Silva, Opt. Mater. 89, 334 (2019).
- J. C. A. Santos, E. P. Silva, D. V. Sampaio, D. C. Silva, N. R. S. Souza,
   C. Kucera, J. Ballato, and R. S. Silva, J. Eur. Ceram. Soc. 40, 3673 (2020).
- A. A. Trofimov, J. C. A. Santos, D. V. Sampaio, R. S. Silva, T. A. DeVol, and L. G. Jacobsohn, J. Lumin. 251, 119206 (2022).
- D. V. Sampaio, N. R. S. Souza, J. C. A. Santos, D. C. Silva, E. J. S. Fonseca, C. Kucera, B. Faugas, J. Ballato, and R. S. Silva, Ceram. Inter. 42, 4306 (2016).
- Y. G. S. Alves, D. V. Sampaio, N. R. S. Souza, D. C. Silva, T. R. Cunha, C. T. Meneses, E. J. S. Fonseca, and R. S. Silva, Opt. Mater. 70, 63 (2017).
- 13) N. R. S. Souza, D. C. Silva, D. V. Sampaio, M. V. S. Rezende, C. Kucera, A. A. Trofimov, L. G. Jacobsohn, J. Ballato, and R. S. Silva, Opt. Mater. 68, 2 (2017).
- 14) Y. G. S. Alves, D. V. Sampaio, J. C. A. Santos, M. V. S. Rezende, N. R. S. Souza, C. Kucera, J. Ballato, and R. S. Silva, Optik 221, 165 (2020).
- D. C. Silva, A. S. Lima, J. H. L. Silva, M. V. S. Rezende, D. V. Sampaio,
   J. Ballato, and R. S. Silva, J. Eur. Ceram. Soc. 41, 3629 (2021).
- 16) M. Nikl, A. Yoshikawa, K. Kamada, K. Nejezchleb, C. R. Stanek, J. A. Mares, and K. Blazek, Prog. Crys. Growth Charac. Mater. 59, 47 (2013).
- 17) R. D. Shannon, Acta Cryst. A 32, 751 (1976).
- H. Ogino, A. Yoshikawa, M. Nikl, K. Kamada, and T. Fukuda, J. Crys. Growth 292, 239 (2006).
- M. R. Marchewka, M. G. Chapman, H. Qian, and L. G. Jacobsohn, Opt. Mater. 68, 53 (2017).
- A. A. Trofimov, M. R. Marchewka, and L. G. Jacobsohn, Rad. Meas. 122, 34 (2019).
- P. A. Cutler, C. L. Melcher, M. A. Spurrier, P. Szupryczynski, and L. A. Eriksson, IEEE Trans. Nucl. Sci. 56, 915 (2009).

- J.-J. Song, P. B. Klein, R. L. Wadsack, M. Selders, S. Mroczkowski, and R. K. Chang, J. Opt. Soc. Am. 63, 1135 (1973).
- G. Mace, G. Schaack, N. Toaning, and J. A. Koningstein, Z. Physik 230, 391 (1970).
- 24) M. Nikl, H. Ogino, A. Krasnikov, A. Beitlerova, A. Yoshikawa, and T. Fukuda, Phys. Status Solidi a 202, R4 (2005).
- 25) A. M. Srivastava, J. Lumin. 169, 445 (2016).
- W. Drozdowski, P. Dorenbos, R. Drozdowska, A. J. J. Bos, N. R. J. Poolton, M. Tonelli, and M. Alshourbagy, IEEE Trans. Nucl. Sci. 56, 320 (2009).
- P. Gluchowski, R. Pazik, D. Hreniak, and W. Strek, J. Lumin. 129, 548 (2009).
- 28) A. A. Trofimov, C. Li, K. S. Brinkman, and L. G. Jacobsohn, Opt. Mater. 68, 7 (2017).
- 29) J.-P. Zhong, H.-B. Liang, Q. Su, J.-Y. Zhou, and J.-Y. Wang, Trans. Nonferr. Metal Soc. 19, 1628 (2009).
- 30) J. Pejchal et al., Opt. Mater. 53, 54 (2016).
- S. Liu, X. Feng, M. Nikl, L. Wu, Z. Zhou, J. Li, H. Kou, Y. Zeng, Y. Shi, and Y. Pan, J. Am. Cer. Soc. 98, 510 (2015).
- 32) V. T. Gritsyna, Y. G. Kazarinov, V. A. Kobyakov, and I. E. Reimanis, Nucl. Instrum. Methods Phys. Res. B 250, 342 (2006).
- 33) O. K. Tyutyunik, A. O. Moskvitin, Y. G. Kazarinov, and V. T. Gritsyna, Funct. Mater. 17, 41 (2010).



Luiz G. Jacobsohn received the D.Sc. degree in physics from the Pontifical Catholic University of Rio de Janeiro, Brazil, in 1999. He joined Los Alamos National Laboratory in 2002 as a post-doctoral research associate, and in 2005 was converted to technical staff member. In 2009, he joined Clemson University's Department of Materials Science and Engineering as a research faculty. Presently, he is an associate professor with the same Department. He is the recipient of the National Science Foundation CAREER award in 2017 and the U.S. Fulbright Scholar

award in 2022. His research interests involve scintillators, luminescence dosimeters, and luminescent materials in general. Presently, he is on sabbatical leave at LumiLab with Ghent University, Belgium.



Robin Conner received a Bachelor's degree Magna Cum Laude in physics from Clemson University in 2022. She joined Dr. Jacobsohn's research group in 2021 focusing on synthesizing, processing, and characterizing luminescent materials. Currently, she is pursuing her Master's degree in Materials Science and Engineering at Clemson University examining the microstructure, defects, and luminescence of spinels.



Ronaldo Silva has been a professor with the Department of Physics of the Federal University of Sergipe (UFS), Brazil, since 2009 and is currently the Coordinator of the Graduate Program in physics. He is also adjunct professor with the Department of Materials Science and Engineering (MSE) of Clemson University, USA. He received a Bachelor's and a Master's degree in physics from UFS in 2000 and 2003, respectively, and a D.Sc. in applied physics from IFSC-USP in 2006. He was a business post-doctoral (PDI) fellow with Cerâmica Sergipe S/

A within 2007–2009, and a post-doctoral fellow with Clemson University's MSE Department within 2017–2018. His expertise is in condensed matter physics and technology transfer to industry, and he is working on the production of new ceramics, luminescent, dielectric, and ferroelectric materials, as well as with scientific instrumentation.